

Synthesis, investigation on structural and electrical properties of cobalt doped Mn–Zn ferrite nanocrystalline powders

M. BHUVANESWARI¹, S. SENDHILNATHAN^{2*}, M. KUMAR³, R. TAMILARASAN⁴,
N.V. GIRIDHARAN⁵

¹Department of Physics, Mount Zion College of Engineering and Technology, Pudukkottai-622507, India

²Department of Physics, Anna University Chennai: University College of Engineering-Pattukkottai,
Rajamadam-614701, India

³Department of Chemistry, Easwari Engineering College, Ramapuram, Chennai-600089, India

⁴Department of Chemistry, Anna University Chennai: University College of Engineering-Pattukkottai,
Rajamadam-614701, India

⁵Advanced Functional Materials Laboratory, Department of Physics, National Institute of Technology,
Tiruchirappalli-620015, India

Synthesis of $\text{Co}_x\text{Mn}_y\text{Zn}_y\text{Fe}_2\text{O}_4$ ($x = 0.1, 0.5, 0.9$ and $y = 0.45, 0.25, 0.05$) nanocrystalline powders was done by chemical co-precipitation method. The crystal structure was determined by using X-ray diffraction (XRD) studies. The crystallite size and lattice parameters were calculated from the XRD data. The XRD results revealed that the crystallite size of the nanocrystalline powder was found to decrease from 37 nm to 28 nm with the substitution of cobalt. The effect of cobalt ions on the crystallization process, the lattice parameters and electrical properties of Mn–Zn ferrites has been also investigated. The AC conductivity increased with an increase in frequency but it decreased with an increase in cobalt content. The complex impedance analysis of the data showed that the resistive and capacitive properties of the Co–Mn–Zn ferrite are predominant due to the fact that the processes are associated with the grains and grain boundaries. The dielectric constant and dielectric loss dependence on doping level and frequency at room temperature were also studied.

Keywords: *nanoferrites; cobalt substituted Mn–Zn ferrite; Co-precipitation; magnetic nanoparticle; dielectric constant*

© Wroclaw University of Technology.

1. Introduction

Cobalt doped ferrites (CoFe_2O_4) have been extensively studied because of their excellent unique properties, such as cubic magneto-crystalline anisotropy, high coercivity, moderate saturation-magnetization, high chemical stability, wear resistance and electrical insulation property [1, 2]. Even though the magnetic materials are quite old and well-studied, they have experienced a renewed interest in recent years in the context of microwave industry, disk recording, refrigeration systems, electrical devices, transformers, frequency filters, sensors, pigments, and medical applications, such as cancer treatment by hyperthermia, MRI

contrast agent, drug delivery, DNA hybridization and cell separation [3]. Cobalt doped ferrites having unique high chemical stability and high electrical resistivity caused that the magnetic ceramics or ferrites with the spinel structure have received special attention [4]. Ferrites can be represented by the chemical formula of AB_2O_4 , where A and B denote metal cations at tetrahedral (A) and octahedral (B) sites, respectively. The magnetic properties of the spinel ferrite materials originate from the anti-ferromagnetic coupling between the octahedral and tetrahedral sublattices [5].

Cobalt doped ferrite is a material which is suitable for non-contact stress sensor applications. It possesses some specific properties, such as large strain derivative good corrosion resistance, no eddy current loss and low cost (rare-earth free) [6].

*E-mail: senthil29@yahoo.com

Nevertheless, some of their properties can be manipulated not only by choosing a suitable doping material (to form a ternary cation spinel) but also by choosing a suitable synthesis method. The spinel ferrites have been synthesized by different methods such as ceramic process, co-precipitation method, hydrothermal process, sol-gel synthesis and micro-emulsion approach. The chemical co-precipitation method seems to be the most convenient method because it allows firing powders with good chemical homogeneity and small grain sizes. It allows a good control of their shape and size distribution due to the components mixed at a molecular level during nanopowder synthesis. Having these above advantages, the chemical co-precipitation method is an emerging popular process to synthesize ferrite nanopowders. Ferrites have important characteristic properties, such as high resistivity and low eddy current losses [7], which make them ideal for high frequency applications. Owing to the dielectric behavior, they are sometimes called multiferroics. They are also commercially important materials because they are widely used in microwave devices (which utilize the nonreciprocity of ferrites) such as circulators, isolators, phase shifters, and antennas. Circulators were developed for radar systems and are now used in mobile phones. They allow the use of the same device for transmission and reception of the response signal. Miniaturization and weight reduction in mobile communication devices requires small and thin, film-type isolators [8].

In the literature, synthesis and investigation of magnetic properties of spinel cobalt doped Mn–Zn ferrites nanoparticles has been carried out by several workers. The large number of researchers has reported magnetic properties of cobalt doped ferrite nanopowders with a view to understand magnetism at nanoscale and their possible practical applications. However, much less attention has been paid to study the electrical properties of cobalt doped ferrite nanopowders. Gabal et al. [9] reported the structural, electrical and magnetic properties of aluminum substituted Mn–Zn ferrites nanopowders prepared via sol-gel auto-combustion method. The investigations of electrical properties of cobalt

doped ferrite nanopowders are important from the point of view of their use in electrical and electronic industry applications. Gagan et al. [10] studied electrical and dielectric properties of cobalt substituted Mg–Mn nanoferrites synthesized by solution combustion technique.

In the present work, the $\text{Co}_x\text{Mn}_y\text{Zn}_y\text{Fe}_2\text{O}_4$ nano powders ($x = 0.1, 0.5, 0.9$ and $y = 0.45, 0.25, 0.05$) were synthesized by chemical co-precipitation method and the consequent change in particle size, dielectric behavior at room temperature were reported. Further, the structural and electrical properties of the cobalt doped Mn–Zn ferrite nanopowders were studied. The electrical parameters such as dielectric strength, dielectric dissipation factor were obtained.

2. Materials and methods

The cobalt doped Mn–Zn ferrite nanopowders were synthesized by co-precipitation method (Fig. 1). The process depend mostly on parameters such as reaction temperature, pH of the suspension, initial molar concentration, etc. [11]. Ultrafine particles of $\text{Co}_x\text{Mn}_y\text{Zn}_y\text{Fe}_2\text{O}_4$ ($x = 0.1, 0.5, 0.9$ and $y = 0.45, 0.25, 0.05$), CMZF were prepared by co-precipitating aqueous solutions of CoCl_2 , MnCl_2 , ZnCl_2 and FeCl_3 mixtures respectively in an alkaline medium. The mixed solution of CoCl_2 , MnCl_2 , ZnCl_2 and FeCl_3 in respective proportions (100 mL of 0.1 M CoCl_2 , 100 mL of 0.45 M ZnCl_2 , 100 mL of 0.45 M MnCl_2 and 100 mL of 2 M FeCl_3 in case of $\text{Co}_{0.1}\text{Mn}_{0.45}\text{Zn}_{0.45}\text{Fe}_2\text{O}_4$ and similarly for the other values of x) was prepared and kept at 60 °C.

This mixture was added to a boiling solution of NaOH (0.1 M dissolved in 1200 mL of distilled water) within 10 seconds under constant stirring. The nanoferrites were formed by conversion of metal salts into hydroxides, which took place immediately, followed by the transformation of hydroxides into ferrites. The solutions were maintained at 85 °C for one hour. This duration was sufficient for the transformation of hydroxides into spinel ferrite (dehydration and atomic rearrangement involved in the conversion of intermediate hydroxide phase into ferrite). Sufficient amount of fine

particles was collected at this stage by using magnetic separation method [12]. The particles were washed several times with distilled water followed by acetone and dried at room temperature.

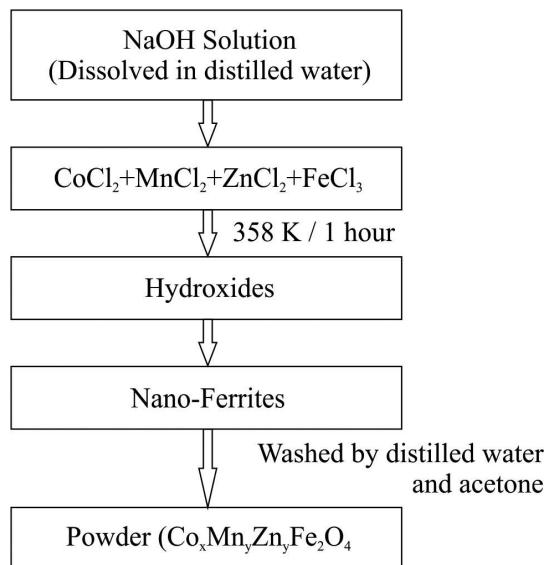


Fig. 1. Flow chart for the preparation of $\text{Co}_x\text{Mn}_y\text{Zn}_y\text{Fe}_2\text{O}_4$ ($x = 0.1, 0.5, 0.9$ and $y = 0.45, 0.25, 0.05$) nanopowders.

2.1. Characterization methods

The crystalline structure of the CMZF nanopowders was examined using BRUKER-binary V2 (RAW) powder diffractometer using $\text{CuK}\alpha$ ($\lambda = 1.54060 \text{ \AA}$) radiation. The surface morphologies of the nanopowders were measured with a scanning electron microscope. For the electrical measurements, the powder sample was pelletized at a pressure of 300 kg/cm^2 to yield a pellet of 10 mm diameter and 2 mm thickness. The dielectric constant and loss tangent of these powders were measured by using LCR HiTESTER (HiOKI 3532-50). The crystalline structure of CMZF nanopowders was determined by using FT-IR spectroscopy.

3. Results and discussion

3.1. Structural analysis

The XRD patterns of $\text{Co}_x\text{Mn}_y\text{Zn}_y\text{Fe}_2\text{O}_4$ ($x = 0.1, 0.5, 0.9$ and $y = 0.45, 0.25, 0.05$)

nanopowders are shown in Fig. 2. The diffraction peaks compared to the standard XRD pattern (PDF# 871171) correspond to (1 1 2), (1 0 3), (2 0 2), (2 1 3), (3 0 3), (2 2 4) and (3 1 4) planes. The peaks detected in the XRD patterns belong to the tetragonal structure of spinel ferrite and confirm the lack of formation of any secondary phase [13]. Fig. 3 shows that the peaks are shifted to higher angles with an increase in cobalt concentration in the Mn–Zn ferrite. The peak position was found to shift towards higher diffraction angles due to the smaller ionic radius of cobalt (0.938 \AA) compared to Mn and Zn radius.

XRD analysis can also be used to evaluate peak broadening with crystallite size, and lattice strain due to dislocations [14]. The crystallite sizes of the $\text{Co}_x\text{Mn}_y\text{Zn}_y\text{Fe}_2\text{O}_4$ samples found using Debye-Scherrer formula (equation 1) were 35 nm, 37 nm and 28 nm at $x = 0.1, 0.5$ and $x = 0.9$, respectively:

$$D = \frac{k\lambda}{\beta_{hkl} \cos \theta} \quad (1)$$

where D is the crystallite size, k is the shape factor ($k = 0.9$), λ is the wavelength of $\text{CuK}\alpha$ radiation and β_{hkl} is the instrument corrected integral breadth of the reflection (in radians) located at 2θ , and θ is the angle of reflection (in degrees).

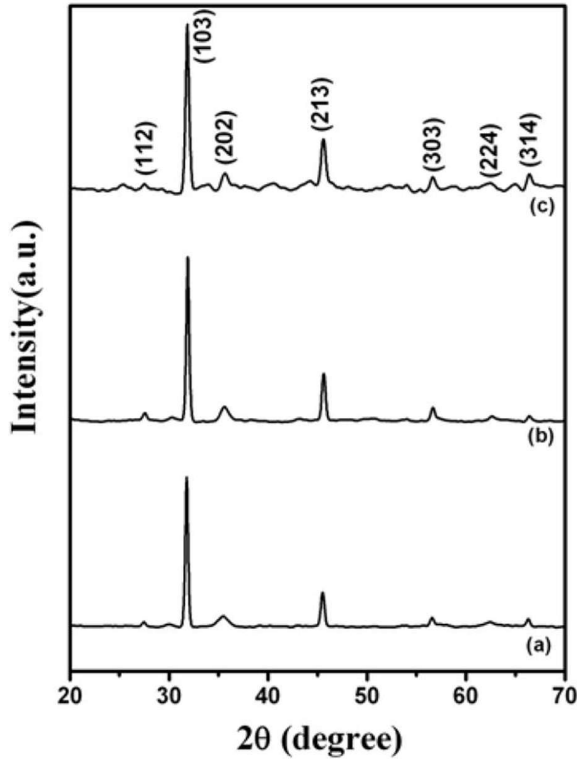
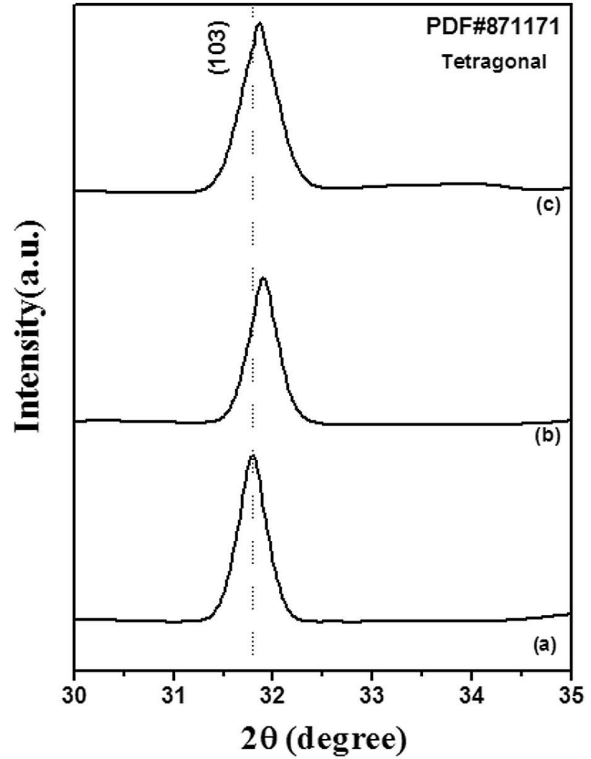
The values of lattice parameters of $\text{Co}_x\text{Mn}_y\text{Zn}_y\text{Fe}_2\text{O}_4$ nanopowders were calculated and listed in Table 1.

The values were compared with the standard values of Mn–Zn ferrite. The ratio of c/a had the value greater than unity, attributed to a tetragonal structure. Fig. 4. shows the graphical representation of lattice parameter values with respect to enhancement in cobalt content in the Mn–Zn ferrite. The lattice parameter values were found to increase with increasing cobalt content up to $x = 0.5$. Upon further increase in the cobalt content, the value decreased due to the density of cobalt in the unit cell. This behavior was confirmed by the volume of unit cell and strain calculation.

The scanning electron micrographs of $\text{Co}_x\text{Mn}_y\text{Zn}_y\text{Fe}_2\text{O}_4$ nanopowders are shown in Fig. 5. It implies that the materials have a well-defined microstructure. The micrographs indicate

Table 1. Lattice constants, strain and crystallite size of $\text{Co}_x\text{Mn}_y\text{Zn}_y\text{Fe}_2\text{O}_4$.

$\text{Co}_x\text{Mn}_y\text{Zn}_y\text{Fe}_2\text{O}_4$	Lattice parameter [Å]			Volume of the unit cell [Å ³]	Strain [ε]	Crystallite size [nm]
	a	b	c			
x = 0.1, y = 0.45	5.556	5.556	9.823	303.20	0.00153	35
x = 0.5, y = 0.50	5.564	5.564	10.402	322.09	−0.000704	37
x = 0.9, y = 0.05	5.508	5.508	10.279	311.81	−0.000851	28


 Fig. 2. X-ray diffraction patterns for $\text{Co}_x\text{Mn}_y\text{Zn}_y\text{Fe}_2\text{O}_4$ with (a) $x = 0.1, y = 0.45$ (b) $x = 0.5, y = 0.25$ and (c) $x = 0.9, y = 0.05$.

 Fig. 3. The magnified XRD patterns of $\text{Co}_x\text{Mn}_y\text{Zn}_y\text{Fe}_2\text{O}_4$ ($x = 0.1, 0.5, 0.9$ and $y = 0.45, 0.25, 0.05$) nanopowders in the range of 30° to 35° .

homogeneous distribution of polycrystalline grains throughout the material. This also indicates that the CMZF nanopowders possess relatively narrow size distribution.

3.1.1. W-H analysis

Since the breadth of the Bragg peak is the combination of both instrumental and sample dependent effects, it is necessary to collect a diffraction pattern from the line broadening of a standard material such as silicon to determine the instrumental broadening [15].

The instrumental corrected broadening β_{hkl} corresponding to the diffraction peak of $\text{Co}_x\text{Mn}_y\text{Zn}_y\text{Fe}_2\text{O}_4$ was estimated from the relation:

$$\beta_{hkl} = [(\beta_{hkl})_{measured}^2 - \beta_{instrumental}^2]^{1/2} \quad (2)$$

Williamson and Hall (W-H) proposed a method of deconvoluting size and strain from the mathematical expression given by:

$$\beta_{hkl} \cos \theta = \left[\frac{k\lambda}{D} \right] + 4\epsilon_s \sin \theta \quad (3)$$

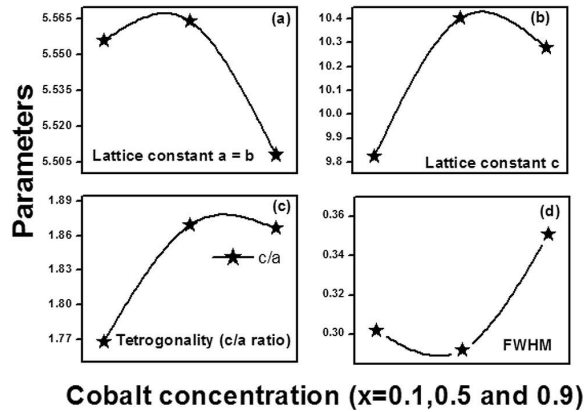


Fig. 4. Variation of lattice constants (a, b), tetragonality (c) and FWHM (d) with cobalt content for the Mn-Zn ferrite nanopowders.

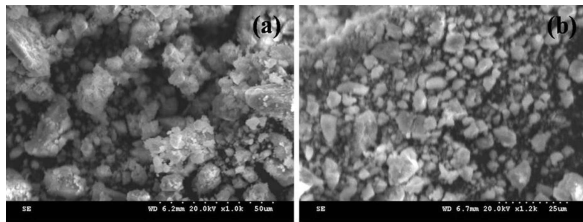


Fig. 5. SEM micrographs of the Mn-Zn ferrite nanopowders doped with cobalt.

where k is the shape factor, λ is the X-ray wavelength, θ is the Bragg angle, D is the effective crystallite size, ε_s is the strain and β_{hkl} is the full width at half maximum of the corresponding (h k l) plane. A plot drawn between $4 \sin\theta$ along the X-axis and $\beta_{hkl} \cos\theta$ along the Y-axis is shown in Fig. 6. From the data of linear fit, the value of strain was calculated from the slope of the line. W-H analysis (equation 3) is a simplified integral-breadth method, where size-induced and strain-induced broadening is deconvoluted by considering the peak width as a function of 2θ [16]. The strain ε was evaluated from the slope of the linear fit and the values were found to be 0.00153 for $x = 0.1$, -0.0007048 for $x = 0.5$ and -0.0008518 for $x = 0.9$ respectively. The strain results show that the strain changes from tensile to compressive nature with the increase in the cobalt content in the Mn-Zn ferrite.

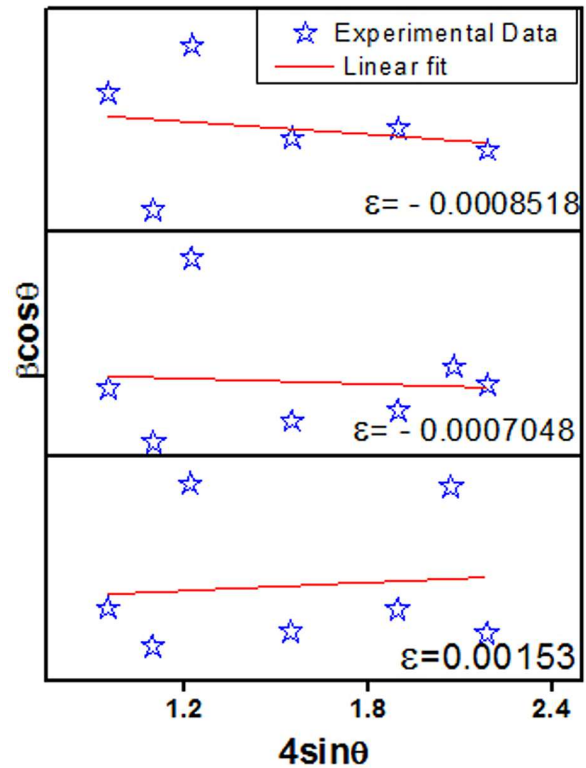


Fig. 6. W-H plot of $\text{Co}_x\text{Mn}_y\text{Zn}_y\text{Fe}_2\text{O}_4$ with (a) $x = 0.1$, $y = 0.45$ (b) $x = 0.5$, $y = 0.25$ and (c) $x = 0.9$, $y = 0.05$.

3.2. Dielectric properties

The dielectric properties of $\text{Co}_x\text{Mn}_y\text{Zn}_y\text{Fe}_2\text{O}_4$ with $x = 0.1, 0.5, 0.9$ and $y = 0.45, 0.25, 0.05$ were studied using HIOKI 3532-50 LCR HITESTER. Dielectric loss, dielectric constant were computed according to Smit and Wijn [17] as a function of frequency. Fig. 7 and Fig. 8 show that the dielectric constant as well as dielectric loss decrease with increasing frequency, exhibiting normal ferrimagnetic behavior for all the compositions. It can be seen that the dielectric constant decreases with increasing frequency in the lower frequency region. As the frequency increases to higher values, the dielectric constant remains almost constant. This is a typical behavior of ferrites and it can be explained with the help of Maxwell-Wagner model [18]. According to this model, ferrites consist of two layers, first of which contains well conducting grains (ferrous ions), and the second one is composed of poorly conducting grain boundaries. These grain

boundaries are more active at lower frequencies; hence, the hopping frequency of electrons between Fe^{3+} and Fe^{2+} ions is less at lower frequencies.

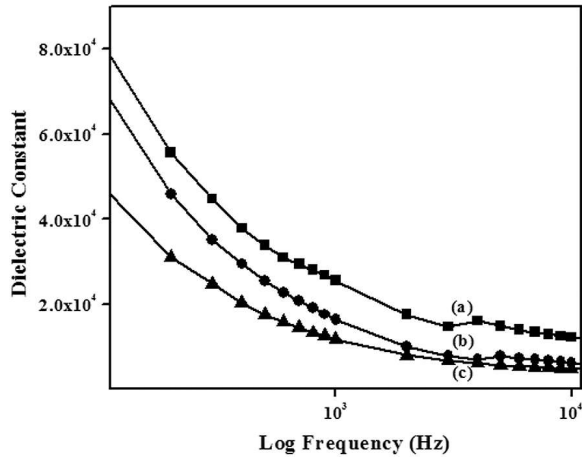


Fig. 7. Variation of dielectric constant with frequency for $\text{Co}_x \text{Mn}_y \text{Zn}_y \text{Fe}_2 \text{O}_4$ with (a) $x = 0.1$, $y = 0.45$ (b) $x = 0.5$, $y = 0.25$ and (c) $x = 0.9$, $y = 0.05$.

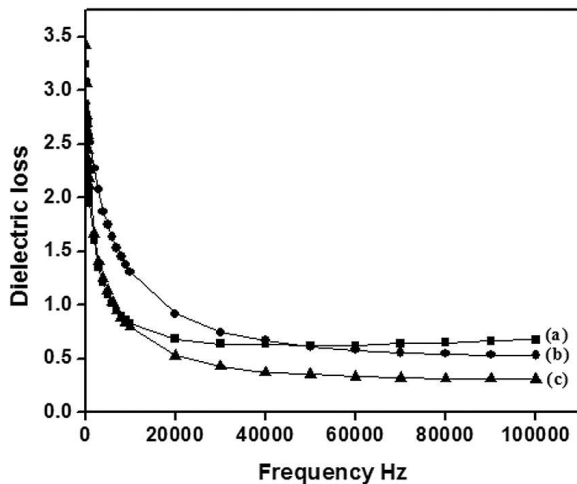


Fig. 8. Variation of dielectric loss with frequency for $\text{Co}_x \text{Mn}_y \text{Zn}_y \text{Fe}_2 \text{O}_4$ with (a) $x = 0.1$, $y = 0.45$ (b) $x = 0.5$, $y = 0.25$ and (c) $x = 0.9$, $y = 0.05$.

The dielectric properties of ferrites cause localized accumulation of charge under the influence of electric field. The polarization in ferrites is similar to the conduction of electrons in Fe^{2+} and Fe^{3+} . At lower frequencies the conduction is favorable and, as a result, the dielectric constant is high but

it continuously decreases with increasing frequency because the electron exchange between Fe^{2+} and Fe^{3+} cannot follow the higher AC field frequency. Largeteau et al. [19] showed that permittivity values are composition dependent and for ferrites containing ferrous ions in excess, the relative real permittivity usually attains values as high as 10^5 to 10^6 for the frequency ranging from 10^2 Hz to 10^5 Hz. The observed permittivity values ϵ' are of the order of 10^4 in the frequency range of 10^2 Hz to 10^3 Hz. The low dielectric values make these ferrites useful in higher frequency applications [20].

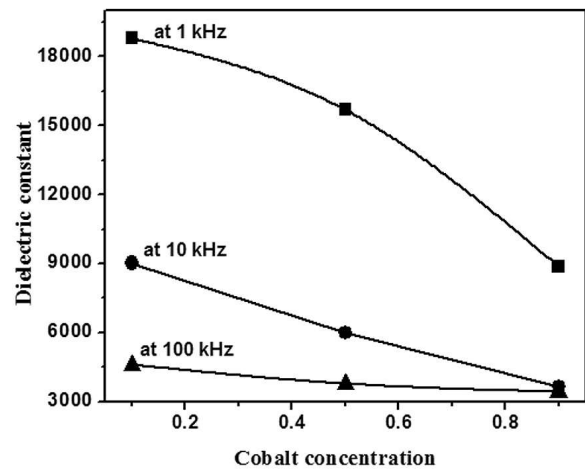


Fig. 9. Variation of dielectric constant with cobalt content for the Mn–Zn ferrite nanopowders.

Fig. 9 shows the variation of dielectric constant with an increase in cobalt concentration at different frequencies (1 kHz, 10 kHz and 100 kHz). The decrease of dielectric constant with cobalt substitution can be explained on the basis of the mechanism of polarization process in ferrites, which is similar to that in the conduction process.

The whole polarization in ferrites is mainly contributed by the space charge polarization which is governed by the number of space charge carriers. The conductivity in materials and the hopping exchange of the charges between two localized states is governed by density of the localized states and the displacement of the charges with respect to the external field. The addition of cobalt ions reduces the iron ions in B-sites, which is mainly responsible for both space charge polarization and

hopping exchange between the localized states. Therefore, the increase in cobalt content causes a decrease in polarization which is accomplished by a decrease of dielectric constant, ϵ' , of the composition. Koops *et al.* [21] suggested that the effect of grain boundaries is predominant at lower frequencies. The thinner grain boundary, the higher the dielectric constant. The decrease in dielectric constant promotes the quality factor at high frequencies. The numerical values for dielectric constants at different frequencies are given in Table 2.

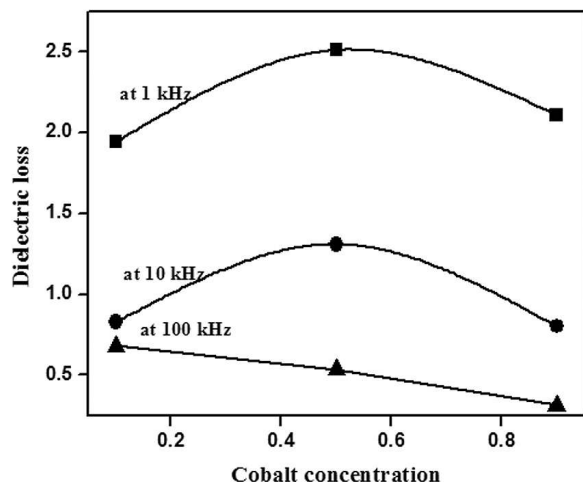


Fig. 10. Variation of dielectric loss with cobalt content for the Mn–Zn ferrite nanopowders.

The variation of dielectric loss tangent with cobalt concentration is shown in Fig. 10. It is observed that at frequencies 1 kHz and 10 kHz the dielectric loss increases with an increase in cobalt content and then decreases. But at a frequency of 100 kHz the dielectric loss is found to be gradually decreasing.

3.3. AC conductivity

The AC conductivity of the material is frequency dependent. The AC conductivity of the CMZF samples was estimated from the dielectric parameters.

Fig. 11 shows the dependence of AC conductivity on cobalt concentration and frequency of the applied AC field. It suggests that AC conductivity is strongly frequency dependent. It is

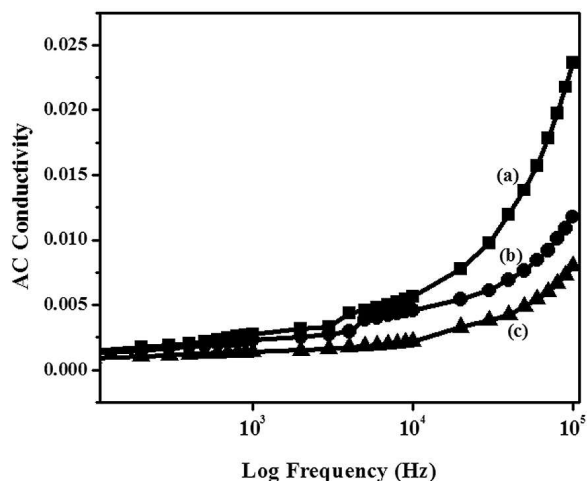


Fig. 11. Variation of AC conductivity with frequency for $\text{Co}_x \text{Mn}_y \text{Zn}_y \text{Fe}_2 \text{O}_4$ with (a) $x = 0.1$, $y = 0.45$ (b) $x = 0.5$, $y = 0.25$ and (c) $x = 0.9$, $y = 0.05$.

evident from the graph that AC conductivity increases with increasing frequency. The conduction mechanism in ferrites can be explained on the basis of hopping of charge carriers between Fe^{2+} – Fe^{3+} ions in octahedral sites [22]. The AC conductivity of a system depends on the dielectric properties and capacitance of the material. The variation of AC conductivity of CMZF indicates the conductivity dispersion throughout the range of frequency under investigation. This behavior may be attributed to the presence of space charge in the material [23]. The doping of CMZF with different concentrations of cobalt results in the modification of the conductivity spectrum. Further, it is observed that as cobalt content increases the AC conductivity decreases.

3.4. Impedance spectroscopy

Impedance spectroscopy is an important method to study the electrical properties of ferrites as the impedance of grains can be separated from the other impedance sources, such as impedance of electrodes and grain boundaries. One of the most important factors which influences the impedance properties of ferrites is the micro structural effect. The impedance measurement gives us information about the resistive (real part) and reactive

Table 2. Dielectric constants at different frequencies.

Samples	Dielectric constant		
	at 1kHz	at 10 kHz	at 100 kHz
$\text{Co}_{0.1}\text{Mn}_{0.45}\text{Zn}_{0.45}\text{Fe}_2\text{O}_4$	18785.8572	9017.0618	4599.6196
$\text{Co}_{0.5}\text{Mn}_{0.25}\text{Zn}_{0.25}\text{Fe}_2\text{O}_4$	15679.6318	5982.7864	3769.3166
$\text{Co}_{0.9}\text{Mn}_{0.05}\text{Zn}_{0.05}\text{Fe}_2\text{O}_4$	8877.4788	3644.987	3422.8054

(imaginary part) components of a material. The impedance behavior can be described by Debye's formula for a serial-parallel resistor-capacitor (RC) circuit with elements that correspond to the dielectric behavior of different components [24]. The complex impedance response commonly exhibits semicircular forms in the measured Cole-Cole plot as shown in Fig. 12.

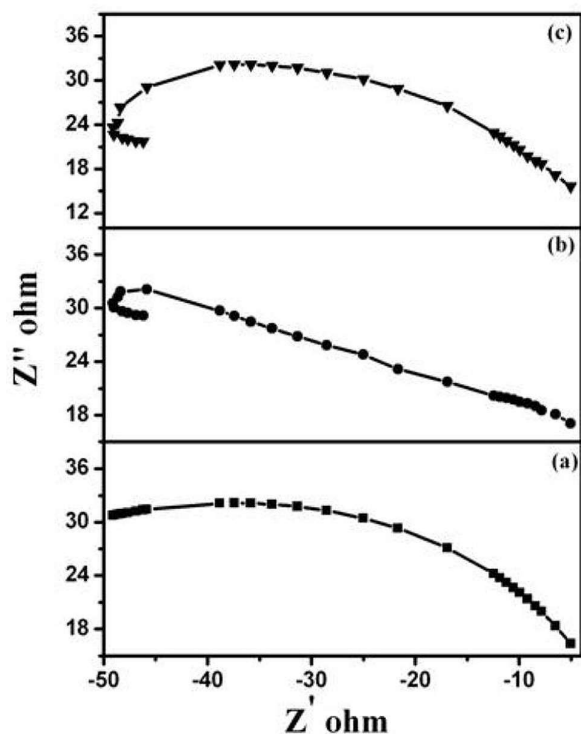


Fig. 12. Cole-Cole plot for $\text{Co}_x\text{Mn}_y\text{Zn}_y\text{Fe}_2\text{O}_4$ with (a) $x = 0.1$, $y = 0.45$ (b) $x = 0.5$, $y = 0.25$ and (c) $x = 0.9$, $y = 0.05$.

It is evident that a single semicircle is seen for all the compositions, however, the semicircle appears to be smaller for the composition $\text{Co}_{0.5}\text{Mn}_{0.25}\text{Zn}_{0.25}\text{Fe}_2\text{O}_4$. Decentralization

of the semicircles has been observed in compositions of Mn ferrite [25]. The grain-boundary resistance is normally higher than the grain interior and the probing interface resistance is higher than that of the boundary. The larger radius of the Cole-Cole plot in frequency space corresponds to contribution from a constituent of lower resistance [26]. Therefore, the semicircle can be attributed to the behavior of grain interior.

3.5. FT-IR spectroscopy studies

The FT-IR spectra analysis was carried out with an FT-IR spectrometer, having the resolution of spectral range covering 4000 cm^{-1} to 400 cm^{-1} , range commonly used in a first determination step. The sample pellets were prepared using 100 mg of dry KBr and 2 mg of the obtained $\text{Co}_x\text{Mn}_y\text{Zn}_y\text{Fe}_2\text{O}_4$ nanopowder. The FT-IR spectra of the $\text{Co}_x\text{Mn}_y\text{Zn}_y\text{Fe}_2\text{O}_4$ materials are shown in Fig. 13. The patterns confirm the presence of cobalt ferrite and hydroxides. The peaks at $\sim 3414\text{ cm}^{-1}$ have been assigned to asymmetric and symmetric OH stretching vibrations of lattice water. The adsorbed water is featured by the bands at 1690 cm^{-1} assigned to the δ H–O–H bonding mode. The bands at 2924 cm^{-1} are assigned to C–O stretching vibrations. Two bands are observed around of 585 cm^{-1} and around 450 cm^{-1} for all $\text{Co}_x\text{Mn}_y\text{Zn}_y\text{Fe}_2\text{O}_4$ samples. These two vibrations bands correspond to the intrinsic lattice vibrations of octahedral and tetrahedral coordination compounds in the spinel structure, respectively [27]. The different frequency between the characteristic vibrations may be attributed to the long band length of oxygen-metal ions in the octahedral sites and shorter band length of oxygen-metal ions in the tetrahedral sites. The difference in the absorption position in the octahedral and tetrahedral

complexes of $\text{Co}_x\text{Mn}_y\text{Zn}_y\text{Fe}_2\text{O}_4$ crystal is due to the difference in the distance between $\text{Fe}^{3+}-\text{O}^{2-}$ in the octahedral and tetrahedral sites [28]. The XRD results and FT-IR results confirm the presence of impurity free nanocrystalline $\text{Co}_x\text{Mn}_y\text{Zn}_y\text{Fe}_2\text{O}_4$.

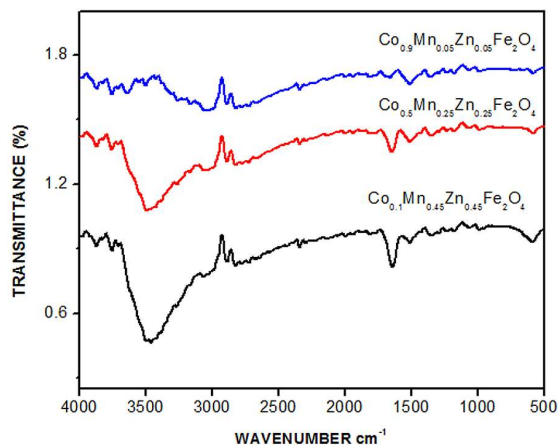


Fig. 13. The FT-IR patterns of $\text{Co}_x\text{Mn}_y\text{Zn}_y\text{Fe}_2\text{O}_4$ with (a) $x = 0.1$, $y = 0.45$ (b) $x = 0.5$, $y = 0.25$ and (c) $x = 0.9$, $y = 0.05$.

4. Conclusions

The nanostructured ferrite $\text{Co}_x\text{Mn}_y\text{Zn}_y\text{Fe}_2\text{O}_4$ ($x = 0.1, 0.5, 0.9$ and $y = 0.45, 0.25, 0.05$) samples were successfully prepared by chemical coprecipitation method. The effect of cobalt doping on the structural and electrical properties of the Mn–Zn ferrite was studied. The XRD analysis showed that the prepared samples had a pure phase tetragonal structure. The higher angle peak shift was observed with an increase in cobalt concentration in Mn–Zn ferrite. The XRD results revealed that the crystallite size of the nanocrystalline powder was found to decrease from 37 nm to 28 nm with the substitution of cobalt. The lattice parameter values increased with increasing the cobalt content up to $x = 0.5$. With a further increase in the cobalt content the values decreased due to the higher density of cobalt in the unit cell. The SEM micrographs indicated that the CMZF nanopowders possessed a relatively narrow size distribution. From the W-H analysis, it was observed that the strain changed from tensile into compressive on increasing the cobalt content in Mn–Zn ferrite. The dielectric constant and dielectric loss were

found to decrease with an increase in cobalt substitution. The permittivity values ϵ' were of the order of 10^4 in the frequency range of 10^2 Hz to 10^3 Hz and decreased to the order of 10^3 with frequency. AC conductivity increased with increasing frequency. It was also observed that as the cobalt content increased the AC conductivity decreased. The resistive and capacitive properties of the Co–Mn–Zn ferrite were discussed using the Cole-Cole plot analysis.

Acknowledgements

The corresponding author, Dr. S. Sendhilnathan, gratefully acknowledges the Department of Science and Technology (Ref. No. SR/FTP/PS-59/2008) for the financial assistance received throughout the project.

References

- [1] RAJENDRAN M., PULLA R.C., BHATTACHARYA A.K., DAS D., CHINTALAPUDI S.N., MAJUMDAR C.K., *J. Magn. Magn. Mater.*, 232 (2001), 71.
- [2] LIU C., ZOU B., RONDINONE A.J., ZHANG Z.J., *J. Amer. Chem. Soc.*, 122 (2000), 6263.
- [3] SHARIFI I., SHOKROLLAHI H., AMIRI S., *J. Magn. Magn. Mater.*, 324 (2012), 903.
- [4] SHOKROLLAHI H., *J. Magn. Magn. Mater.*, 320 (2008), 463.
- [5] MAKOVEC D., KODRE A., ARCON I., DROFENIK M., *J. Nanopart. Res.*, 11 (2009), 1145.
- [6] JILES D.C., LO C.C.H., *Sensor. Actuat. A-Phys.*, 106 (2003), 3.
- [7] YAMAMOTO Y., MAKINO A., *J. Magn. Magn. Mater.*, 133 (1994), 500.
- [8] MARTHA P.H., *J. Magn. Magn. Mater.*, 215 (2000), 171.
- [9] GABAL M.A., ABDEL-DAIEM A.M., AL ANGARI Y.M., ISMAIL I.M., *Polyhedron*, 57 (2013), 105.
- [10] GAGAN K., RITU R., SUCHETA S., KHALID M. B., SINGH M., *Ceram. Int.*, 39 (2013), 4813.
- [11] JEYADEVAN B., CHINNASAMY C.N., SHINODA K., TOHJI K., OKA H., *J. Appl. Phys.*, 93 (2003), 8450.
- [12] SHARIFI I., SHOKROLLAHI H., *J. Magn. Magn. Mater.*, 324 (2012), 2397.
- [13] IBRAHIM S., SHOKROLLAHI H., *J. Magn. Magn. Mater.*, 334 (2013), 36.
- [14] MAKINSON J.D., LEE J.S., MAGNER S.H., DE ANGELIS R.J., WEINS W.N., HIERONYMUS A.S., *Adv. X-ray Anal.*, 42 (2000), 407.
- [15] LEE J.S., DE ANGELIS R.J., *Nanostruct. Mater.*, 7 (1996), 805.
- [16] ZAK A.K., ABD MAJID W.H., ABRISHAMI M.E., YOUSEFI R., *Solid State Sci.*, 13 (2011), 251.
- [17] SMIT J., WIJN H. P. J., *Electrical properties*, in: *Ferrites. Physical properties of ferromagnetic oxides in relation to their technical applications*, Philips technical Library Eindhoven, The Netherlands, 1959, p. 239.

- [18] WAGNER K.W., *Ann. Phys-New York*, 40 (1913), 817.
- [19] LARGETEAU A., RAVEZ J., JACOBS I.S., *Mater. Sci. Eng. B-Adv.*, 8 (1991), 145.
- [20] PATHAN A.T., SHAIKH A.M., *Inter. J. Comp. App.*, 45 (2012), 24.
- [21] KOOPS C.G., *Phys. Rev. Lett.*, 83 (1951), 121.
- [22] SATHISHKUMAR G., VENKATARAJU C., SIVAKUMAR K., *Mater. Sci. App.*, 1 (2010), 19.
- [23] DUTTA S., CHOUDHARY R.N.P., *Appl. Phys. A*, 90 (2008), 323.
- [24] MACDONALD J.R., *Impedance spectroscopy*, Wiley, New York, 1987.
- [25] KHALID M.B., *Physica B*, 406 (2011), 382.
- [26] CHANG Q.S., *Prog. Solid State Ch.*, 35 (2007), 1.
- [27] PUI D.G., CARJA G., *DIG. J. Nanomater. Bios.*, 6 (2011), 1783.
- [28] PAULINE S., PERSIS A.A., *Arch. App. Sci. Res.*, 3 (2011) 213.

Received 2015-08-06

Accepted 2016-02-24